Monte Carlo grain growth modeling with local temperature gradients

2017 Modelling Simul. Mater. Sci. Eng. 25 065003

(http://iopscience.iop.org/0965-0393/25/6/065003)

IOP Publishing Modelling and Simulation in Materials Science and Engineering
Modelling Simul. Mater. Sci. Eng. **25** (2017) 065003 (19pp) https://doi.org/10.1088/1361-651X/aa7327

Monte Carlo grain growth modeling with local temperature gradients

Y Tan[1], A M Maniatty[1], C Zheng[1] and J T Wen[2,3]

[1] Department of Mechanical, Aerospace and Nuclear Engineering, Rensselaer Polytechnic Institute, Troy, NY 12180-3590, United States of America
[2] Department of Industrial and Systems Engineering, Rensselaer Polytechnic Institute, Troy, NY 12180-3590, United States of America
[3] Department of Electrical and Computer Systems Engineering, Rensselaer Polytechnic Institute, Troy, NY 12180-3590, United States of America

E-mail: tany3@rpi.edu

Received 17 January 2017, revised 28 April 2017
Accepted for publication 15 May 2017
Published 7 June 2017

Abstract

This work investigated the development of a Monte Carlo (MC) simulation approach to modeling grain growth in the presence of non-uniform temperature field that may vary with time. We first scale the MC model to physical growth processes by fitting experimental data. Based on the scaling relationship, we derive a grid site selection probability (SSP) function to consider the effect of a spatially varying temperature field. The SSP function is based on the differential MC step, which allows it to naturally consider time varying temperature fields too. We verify the model and compare the predictions to other existing formulations (Godfrey and Martin 1995 *Phil. Mag.* A **72** 737–49; Radhakrishnan and Zacharia 1995 *Metall. Mater. Trans.* A **26** 2123–30) in simple two-dimensional cases with only spatially varying temperature fields, where the predicted grain growth in regions of constant temperature are expected to be the same as for the isothermal case. We also test the model in a more realistic three-dimensional case with a temperature field varying in both space and time, modeling grain growth in the heat affected zone of a weld. We believe the newly proposed approach is promising for modeling grain growth in material manufacturing processes that involves time-dependent local temperature gradient.

Keywords: Monte Carlo, grain growth, site selection probability, temperature gradient

(Some figures may appear in colour only in the online journal)

1. Introduction

Thermal processing plays a critical role in achieving desired engineering properties of metals, which are directly linked to the microstructural characteristics, such as the grain size and shape distribution. During thermal processing, the grain structure evolves through the mechanisms of recrystallization and grain growth. Being able to predict the microstructure resulting from a thermal processing sequence is of great interest, and thus, significant research effort has been devoted to developing models of microstructure evolution resulting from a prescribed thermal history [3]. That effort has primarily focused on the case when the local temperature field is treated as uniform, see for example [4–7]. However, there are cases, such as in the vicinity of a weld or during directional annealing, where the microstructure evolves in the presence of a steep temperature gradient. In the case of a weld, the local temperature gradient is an incidental result of the joining process, which leads to a local gradient in the microstructure that is influenced by the welding process parameters [8, 9]. In the case of directional annealing, a moving local temperature gradient is precisely prescribed to generate elongated grains [10]. With the prospect of being able to generate beneficial local microstructures, there has been recent work to develop a programmable, embedded micro-heater array that can be use to control the temperature distribution across a microscopic sample [11–13]. This paper focuses on the investigation and development of models to predict the microstructure in these cases with local temperature gradients.

One of the most widely used methods to simulate grain growth in metals is the Monte Carlo (MC) method based on the Potts model [4, 5]. In this method a regular lattice is defined, where each lattice point is assigned a grain orientation. A grain is then defined as a collection of lattice points with the same orientation. Evolution of the grain structure is predicted with the following basic procedure: (a) randomly select a lattice point, (b) allow that lattice point to take on a randomly chosen orientation from one of its neighbors, (c) determine if the new orientation is energetically favorable compared to the previous orientation, (d) randomly select between the new or original orientation following a probability associated with the change in energy, and go back to (a) and repeat. One MC step is defined as N_L reorientation attempts, where N_L is the number of lattice points. This procedure and variations on it have been used to model grain growth in the presence of second phase particles [14], anisotropic grain boundary energies [15–18], and abnormal grain growth [19, 20]. These different physical phenomena can be captured by adjusting the energy function in a physically meaningful way, adjusting the probability function associated with reorientation, and inserting the appropriate features, for example particles, into the initial representation of the microstructure.

To consider the effect of variations in temperature, it is first necessary to relate the non-dimensional MC model to the physical dimensions of time, space, and temperature. Radhakrishnan and Zacharia [2] and Gao and Thompson [6] related the evolution in grain size in the MC simulation to theoretical grain growth models in order to relate the MC time step to physical time and temperature. More recently, other researchers have developed methods to scale and calibrate MC simulations with variable grain boundary mobilities by relating to theoretical models [21, 22]. Gao and Thompson [6], noting that experimental studies often show deviations from the ideal theoretical behavior, also used fitting to experimental data to relate the MC time step to physical time and temperature. Several other researchers have used this approach as well [23, 24].

Based on the scaling relationship between the local MC step and physical time and temperature, it is possible to define a strategy in the MC simulation to consider a spatially varying temperature field with time. This may be done by either scaling the local reorientation

probability or by biasing the grid point site selection probability (SSP). Zacharopoulis *et al* [25] scaled the local reorientation probability, related to grain boundary mobility, with a moving Gaussian distribution to simulate directional annealing, however, there was not a direct link to the temperature. Godfrey and Martin [1] linked the local reorientation probability to the temperature to simulate grain growth during directional annealing. Garcia *et al* [26] and Allen *et al* [18] followed a similar approach relating the reorientation probability to the temperature through a temperature dependent mobility. Radhakrishnan and Zacharia [2] first proposed the idea of scaling the probability of selecting each grid site, effectively allowing for the MC step to vary spatially, to model the evolution of the grain structure in a weld heat-affected zone. Other researchers have subsequently adopted the approach of Radhakrishnan and Zacharia [2] to model grain growth in the heat-affected zone near a weld [8, 27, 28].

In this work, starting a scaling relationship where the MC simulation is scaled to physical processes by fitting experimental data, we derive a new grid SSP function to model grain growth when the temperature field varies in space and time. To verify the formulation and to compare to the existing methods described above [1, 2], we test the methods on a simple two-dimensional (2D) domain where the domain split in half at two different constant temperatures. It is expected that each half of the domain will exhibit grain growth following the behavior for a single domain at a constant temperature. After that, a more realistic three-dimensional (3D) test case modeling grain growth in the heat affected zone (HAZ) of a weld is considered, where the temperature field varies in space and time. The predictions of our new formulation are compared to those obtain with the approach of Radhakrishnan and Zacharia [2]. The results are discussed and lastly, conclusions are drawn.

2. Methods

2.1. MC simulation model

In this section, we first expand the basic MC algorithm outlined above and used in this work.

(i) A lattice site i located at position $\boldsymbol{x}_i$, where $i = 1$, N_L and N_L is the total number of lattice points, is selected with a SSP function $P(\boldsymbol{x}_i)$.

(ii) The orientation at the selected lattice site i, denoted S_i^0, is randomly switched to one of its neighbor's orientations S_i^n, where the neighbor is selected with uniform probability, and the change in energy ΔE due to the switch is computed according to

$$\Delta E = J\sum_{j=1}^{N_n}[\delta(S_i^0, S_i^j) - \delta(S_i^n, S_i^j)], \tag{1}$$

where N_n is the number of neighboring lattice sites considered, δ is the Kronecker delta function, which equals one if the orientations compared are the same and zero otherwise. In this work, square lattices considering the first and second nearest neighbors ($N_n = 8$) in 2D and cubic lattices considering first, second, and third nearest neighbors ($N_n = 26$) in 3D are used. The choice of lattice may introduce non-physical anisotropy that can be reduced by increasing the number of nearest neighbor lattice sites and by increasing the simulation temperature [29, 30], which is described in step (iii) below. The specific grain boundary energy is $J = A\sigma\lambda^2$, where σ is the grain boundary energy per unit area, λ is the lattice spacing, and A is a constant that depends on the lattice geometry. Here, the grain boundary energy is treated as isotropic, i.e. independent of the misorientation across the grain boundary.

(iii) The final orientation is selected with a probability function $\check{P}(\Delta E, T(\boldsymbol{x}_i))$ that depends on the change in energy and local temperature $T(\boldsymbol{x}_i)$ at lattice site i. Here, we use a function of the form

$$\check{P}(\Delta E, T(\boldsymbol{x}_i)) = \begin{cases} p_m(T(\boldsymbol{x}_i)) & \text{if } \Delta E \leqslant 0, \\ p_m(T(\boldsymbol{x}_i))\exp\left(-\dfrac{\Delta E}{k_{\mathrm{B}}T_{\mathrm{s}}}\right) & \text{if } \Delta E > 0, \end{cases} \tag{2}$$

where p_m is the probability of switching if the change is energetically favorable, k_{B} is Boltzmann's constant and T_{s} is the simulation temperature, which we note is not the physical temperature T. Increasing the simulation temperature roughens the grain boundaries, which prevents non-physical lattice effects, and slows the rate of grain growth while maintaining parabolic growth. In this work, we set $k_{\mathrm{B}}T_{\mathrm{s}}/J = 0.6634$ in 2D and 5.58 in 3D, which are suggested as optimal by Zöllner [30] for the lattices used in this work.

Each reorientation attempt at site i is considered a local MC step, and the number of local MC steps is denoted $t_{\mathrm{mc}}(\boldsymbol{x}_i)$, which may be spatial varying. We will expand this concept later in section 2.3. A global MC step is associated with N_L reorientation attempts over the whole domain.

2.2. MC model relation to physical grain growth

MC simulations can be scaled to physical processes by fitting experimental data. In MC simulations, the evolution of average grain size $\bar{D}$ follows:

$$\bar{D}^m - \bar{D}_0^m = \lambda^m C t_{\mathrm{mc}}, \tag{3}$$

where λ is the corresponding physical length of the lattice spacing, $\bar{D}_0$ is the initial grain size, and C and m are parameters fitted from simulations. The exponent has been found to be $m = 2$ for isotropic grain boundary energies at long times both in 2D and 3D simulations [7, 25]. Parabolic grain growth ($m = 2$) has also been observed in some MC simulations with anisotropic grain boundary energy [16, 31], although depending on the form of the grain boundary anisotropy, the grain growth exponent has also be observed to vary [16, 32]. Many experimental studies have shown that the following model well captures grain growth physics [33–36]:

$$\bar{D}^n - \bar{D}_0^n = Kt\exp\left(-\frac{Q}{RT}\right), \tag{4}$$

where n, K, t, R, and Q represent the grain growth exponent, growth constant, time, gas constant, and activation energy for grain boundary migration, respectively. By equating the average grain size $\bar{D}$ in equations (3) and (4), the local MC step t_{mc} is related to the physical time t and temperature T.

Equation (4) assumes a constant temperature. If the temperature is changing dynamically in time, the following equation may be used instead [6, 8, 24]

$$\bar{D}^n - \bar{D}_0^n = K\int_0^t \exp\left(-\frac{Q}{RT(t')}\right)\mathrm{d}t' \approx K\sum_{\alpha=1}^{N_t}\exp\left(-\frac{Q}{RT(t_\alpha)}\right)\Delta t_\alpha, \tag{5}$$

where the approximate equation applies a mid-point integration rule with t_α the time at the middle of time step α, Δt_α is the α time increment, and N_t is the total number of time steps at time t.

2.3. Modeling grain growth in a temperature gradient

The effect of a temperature gradient may either be captured by scaling the reorientation probability function $\check{P}$ (specifically, p_m), as done in Godfrey and Martin [1], or scaling the SSP function P, as done in Radhakrishnan and Zacharia [2]. In Godfrey and Martin, the SSP function P is assumed to follow a uniform probability, while the reorientation probability function, p_m in equation (2), is defined as

$$p_m(T(\boldsymbol{x}_i)) = \exp\left(\frac{Q}{RT_{\max}}\right)\exp\left(\frac{-Q}{RT(\boldsymbol{x}_i)}\right), \tag{6}$$

where $T_{\max}$ is the maximum absolute temperature in the simulation domain. Thus, at $T = T_{\max}$, if the system energy is lowered, the reorientation attempt is accepted, and at lower temperatures, it is accepted at a lower probability that decreases exponentially with $1/T$, effectively reducing the grain boundary mobility and slowing grain growth. In Radhakrishnan and Zacharia [2], the SSP function P is assumed to be

$$P(\boldsymbol{x}_i) = \frac{t_{\mathrm{mc}}(T(\boldsymbol{x}_i))}{t_{\mathrm{mc}}(T_{\max})}, \tag{7}$$

where the local MC step t_{mc} is linked to the local temperature, for example using equations (3) and (4). Here, the local MC step can now be thought of as the expected number of reorientation attempts at lattice site i. The reorientation probability $\check{P}$ does not depend on the local physical temperature, as the temperature dependence is captured in the SSP. This approach reduces the number of reorientation attempts in regions where the temperature is lower by reducing the probability of selecting those lattice sites for consideration. Thus, this method is more computationally efficient as it avoids steps (ii) and (iii) in the algorithm outlined in section 2.1 for lattice points at lower temperatures that have a lower probability of reorienting.

Here, we will focus on defining the SSP function P that is consistent with equations (3) and (4). We choose to focus on the SSP function P instead of the reorientation probability $\check{P}$ because it is a more computationally efficient approach and is effectively the same since the overall probability for reorientation at any given site is related to the product of P and $\check{P}$, and thus, scaling either of these by a defined scaling relationship will give the same result. Thus to be consistent, when we compare our work to that of Godfrey and Martin [1], we modify the Godfrey and Martin algorithm so that the SSP P is taken as the function defined in equation (6) rather than p_m. In this work, we set $p_m = 1$ in equation (2), so once a site is selected and the change in energy associated with reorientation computed, the reorientation is accepted if the energy is reduced. The temperature dependent grain growth behavior is captured entirely in the SSP function. Lastly, we also note that while the evolution of the grain structure is not affected by whether the SSP function P or the reorientation probability function $\check{P}$ is scaled, the number of local MC steps t_{mc}, as defined here, will not be the same in these two cases. If the scaling is done on $\check{P}$ rather than P, t_{mc} (the expected number of reorientation attempts) would be the same everywhere because the SSP would be uniform. The following derivation is based on scaling the SSP function P.

Equating the average grain size $\bar{D}$ in equations (3) and (4) and raising to the physical grain growth exponent n yields

$$\lambda^n\left[\left(\frac{\bar{D}_0}{\lambda}\right)^m + Ct_{\mathrm{mc}}\right]^{\frac{n}{m}} = \bar{D}_0^n + Kt\exp\left(\frac{-Q}{RT}\right). \tag{8}$$

Taking a temporal differential increment, we can now relate a differential MC step $\mathrm{d}t_{\mathrm{mc}}$ to a differential physical time increment $\mathrm{d}t$

$$\frac{n}{m}\lambda^n\left[\left(\frac{\bar{D}_0}{\lambda}\right)^m + Ct_{\mathrm{mc}}\right]^{\frac{n}{m}-1} C\ \mathrm{d}t_{\mathrm{mc}} = K\exp\left(\frac{-Q}{RT}\right)\mathrm{d}t. \tag{9}$$

Although we did not consider a temporally changing temperature in the above derivation, if we substituted equation (5) in (8) instead of (4), we would still arrive at equation (9). Solving the above equation for the differential MC step $\mathrm{d}t_{\mathrm{mc}}$, and separating the terms that are spatially dependent from those that are spatially independent, we obtain

$$\mathrm{d}t_{\mathrm{mc}}(\boldsymbol{x}) = \underbrace{\mathrm{d}t\cdot\frac{mK}{nC\lambda^n}}_{\boldsymbol{x}\text{ independent}}\cdot\underbrace{\frac{\exp\left(-\frac{Q}{RT(\boldsymbol{x})}\right)}{\left[\left(\frac{\bar{D}_0}{\lambda}\right)^m + Ct_{\mathrm{mc}}(\boldsymbol{x})\right]^{\frac{n}{m}-1}}}_{\boldsymbol{x}\text{ dependent}}. \tag{10}$$

Hence,

$$\mathrm{d}t_{\mathrm{mc}}(\boldsymbol{x}) \propto \frac{\exp\left(-\frac{Q}{RT(\boldsymbol{x})}\right)}{\left[\left(\frac{\bar{D}_0}{\lambda}\right)^m + Ct_{\mathrm{mc}}(\boldsymbol{x})\right]^{\frac{n}{m}-1}}. \tag{11}$$

If we consider any physical time interval $\mathrm{d}t$, the local differential MC time step $\mathrm{d}t_{\mathrm{mc}}(\boldsymbol{x})$ within $\mathrm{d}t$ for a lattice point at $\boldsymbol{x}$ should be proportional to the number of site selections $\hat{N}(\boldsymbol{x})$ at that lattice point, such that

$$\frac{\mathrm{d}t_{\mathrm{mc}}(\boldsymbol{x})}{[\mathrm{d}t_{\mathrm{mc}}(\boldsymbol{x})]_{\max}} = \frac{\hat{N}(\boldsymbol{x})}{[\hat{N}(\boldsymbol{x})]_{\max}}, \tag{12}$$

where $[\hat{N}(\boldsymbol{x})]_{\max}$ is the maximum number of times any lattice site is selected within the increment $\mathrm{d}t$ across the domain. Let $\boldsymbol{x}^*$ be the lattice location where the right-hand side of equation (11) is a maximum, and thus $[\hat{N}(\boldsymbol{x})]_{\max} = \hat{N}(\boldsymbol{x}^*)$.

By definition, the SSP function is

$$P(\boldsymbol{x}) \equiv \frac{\hat{N}(\boldsymbol{x})}{\hat{N}(\boldsymbol{x}^*)}. \tag{13}$$

Substituting equations (11) and (12) into (13), we obtain the SSP function for a lattice point at $\boldsymbol{x}$

$$P(\boldsymbol{x}) = \frac{\exp\left(-\frac{Q}{RT(\boldsymbol{x})}\right)}{\exp\left(-\frac{Q}{RT(\boldsymbol{x}^*)}\right)}\cdot\frac{\left[\left(\frac{\bar{D}_0}{\lambda}\right)^m + Ct_{\mathrm{mc}}(\boldsymbol{x}^*)\right]^{\frac{n}{m}-1}}{\left[\left(\frac{\bar{D}_0}{\lambda}\right)^m + Ct_{\mathrm{mc}}(\boldsymbol{x})\right]^{\frac{n}{m}-1}}. \tag{14}$$

The probability functions of Godfrey and Martin [1] and Radhakrishnan and Zacharia [2] can be shown to be special cases of the more general SSP function in equation (14).

In some cases, the MC and physical grain growth exponents are equal, $n = m$. In this case, equation (14) reduces to

$$P(\boldsymbol{x}) = \frac{\exp\left(-\frac{Q}{RT(\boldsymbol{x})}\right)}{\exp\left(-\frac{Q}{RT(\boldsymbol{x}^*)}\right)} = \exp\left(\frac{Q}{RT(\boldsymbol{x}^*)}\right)\exp\left(-\frac{Q}{RT(\boldsymbol{x})}\right) \tag{15}$$

which matches the Godfrey and Martin function in equation (6), where $\boldsymbol{x}^*$ is now at the location where $\exp(-Q/RT(\boldsymbol{x}))$ is a maximum, which coincides with the location where $T = T_{\max}$. Furthermore, when $n = m$, equation (8) simplifies to

$$C\lambda^n t_{\mathrm{mc}} = Kt\exp\left(-\frac{Q}{RT}\right) \tag{16}$$

and substituting into equation (15), we obtain

$$P(\boldsymbol{x}) = \exp\left(\frac{Q}{RT(\boldsymbol{x}^*)}\right)\exp\left(-\frac{Q}{RT(\boldsymbol{x})}\right) = \frac{t_{\mathrm{mc}}(\boldsymbol{x})}{t_{\mathrm{mc}}(\boldsymbol{x}^*)} \tag{17}$$

which matches the SSP of Radhakrishnan and Zacharia in equation (7), where $\boldsymbol{x}^*$ is now the lattice site where t_{mc} is a maximum which coincides with the location where $T = T_{\max}$, assuming the temperature field does not change with time. If the temperature field is time dependent, this may no longer hold.

An approximation that is sometimes made is to assume $\bar{D} \gg \bar{D}_0$, which is true after the grains have grown considerably, at large t_{mc}. When this approximation is made, equations (3) and (4) reduce to

$$\bar{D} \approx \lambda(Ct_{\mathrm{mc}})^{\frac{1}{m}}, \quad \bar{D}^n \approx Kt\exp\left(-\frac{Q}{RT}\right). \tag{18}$$

Note that the second equation above, is only true if the temperature field is not time varying. Combining the above equations, we can obtain,

$$\exp\left(-\frac{Q}{RT}\right) \approx \frac{\lambda^n}{Kt}(Ct_{\mathrm{mc}})^{\frac{n}{m}}. \tag{19}$$

Substituting into equation (14), and again assuming small $\bar{D}_0$, we obtain

$$P(\boldsymbol{x}) \approx \frac{\frac{\lambda^n}{Kt}[Ct_{\mathrm{mc}}(\boldsymbol{x})]^{\frac{n}{m}}[Ct_{\mathrm{mc}}(\boldsymbol{x}^*)]^{\frac{n}{m}-1}}{\frac{\lambda^n}{Kt}[Ct_{\mathrm{mc}}(\boldsymbol{x}^*)]^{\frac{n}{m}}[Ct_{\mathrm{mc}}(\boldsymbol{x})]^{\frac{n}{m}-1}} = \frac{t_{\mathrm{mc}}(\boldsymbol{x})}{t_{\mathrm{mc}}(\boldsymbol{x}^*)} \tag{20}$$

which matches the SSP of Radhakrishnan and Zacharia in equation (7), where $\boldsymbol{x}^*$ is now the lattice site where t_{mc} is a maximum.

Thus, equation (14) reduces to the probability functions of both Godfrey and Martin [1] and Radhakrishnan and Zacharia [2] when the grain growth exponent of the simulation matches the physical grain growth exponent, $m = n$, and, in the case of Radhakrishnan and Zacharia [2], when the temperature field is not time dependent. The SSP function (14) also reduces to the probability function of Radhakrishnan and Zacharia [2] after the grains have grown considerably, when $\bar{D} \gg \bar{D}_0$, and when the temperature field is not time varying. The main difference between the SSP derived here from that of Radhakrishnan and Zacharia [2] is that it is evaluated based on the differential MC step, equation (12) rather than the accumulated current MC step, which allows it to properly account for time dependent temperature fields.

In this work, we have limited the investigation to considering only isotropic grain boundary energy and mobility to demonstrate the approach. We have also ignored the temperature dependence of the grain boundary energy σ. The temperature dependence of the grain boundary mobility is captured by the temperature dependent SSP function P. This

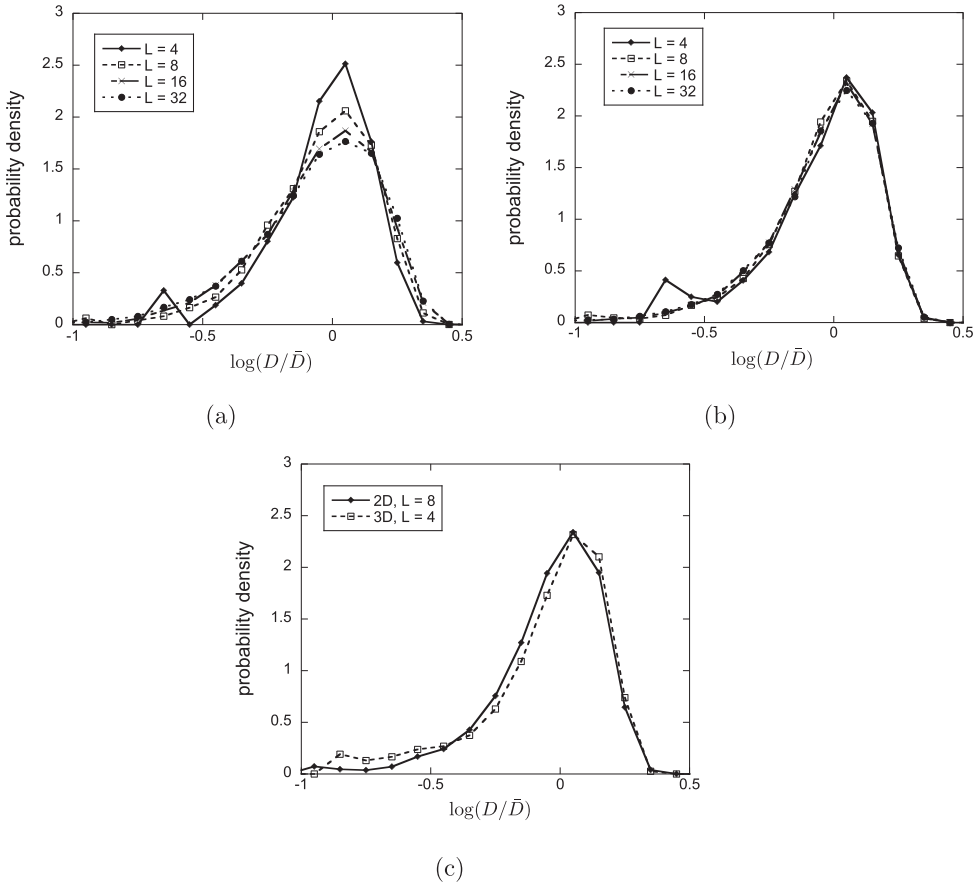

Figure 1. Normalized grain size distributions for MC grown grains grown to different average intercept distances L. (a) 2D results at $T_s = 0$. (b) 2D results at $T_s = 0.6634J/k_B$. (c) 2D and 3D grain size distributions of initial microstructures used in this work with average intercept distances $L = 8$ and $T_s = 0.6634J/k_B$ for 2D simulations and $L = 4$ and $T_s = 5.58J/k_B$ for 3D simulations. Here, D is the grain size on individual grains computed from the square root of the area in 2D and the cube root of the area in 3D.

approach could be combined with methods to consider grain boundary anisotropy, where the grain boundary energy and mobility depend on the misorientation across the grain boundary, and a temperature dependent grain boundary energy. An anisotropic, temperature dependent grain boundary energy would change the form of equation (1) for ΔE and the form of p_m in equation (2), see for example [32], however the rest of the algorithm would remain the same.

Because equation (4) is central to scaling the MC method to physical grain growth, this method is only valid if equation (4) holds. For example, this method is not suitable for modeling recrystallization.

3. Test cases and discussion

The temperature dependent MC model described above was implemented in parallel with an algorithm similar to that described in Wright *et al* [37] based on code developed in the Mesoscale Microstructure Simulation Project [38]. The simulations reported here are run on an IBM Blue Gene/Q.

To test the effect of the different probability functions described in the preceding section, three test cases are investigated. The first two test cases are simple 2D test cases designed to verify the method and to demonstrate how the proposed SSP performs relative to those of Godfrey and Martin [1] and Radhakrishnan and Zacharia [2]. We consider two different materials, copper where $m \approx n = 2$ and aluminum-4%copper with $m \neq n$. The third test case demonstrates the algorithm with a more practical, realistic simulation in 3D predicting the microstructure in the heat-affected zone of a welding process. For the 2D test cases, square lattices are used and the eight nearest neighbor lattice sites are used in computing the energy change in equation (1), and for the 3D case a cubic lattice considering 26 nearest neighbors is used. In each case, the boundaries are treated as mirrored. Before introducing the three cases, we briefly discuss using the MC model to generate an initial representative microstructure.

3.1. Initial microstructure generation

In this work, the simulations are initialized with microstructures close to that resulting from normal grain growth. In normal grain growth, the grain size distribution statistics scale with the grain size, and thus, at different grain sizes the distribution is self-similar [39, 40]. The starting microstructure only has a large impact in the early stages of the MC simulation as the microstructure will naturally evolve towards a self-similar distribution [40]. Thus, starting with a microstructure that is close but not fully evolved to a self-similar distribution will not have a very large impact. It is common in MC simulations to start from a microstructure where each lattice site is identified as a grain [1, 7, 8, 28]. However, that represents a material where all the grains are the same size and is not a realistic microstructure. A more realistic starting microstructure may be created by running a MC simulation on an arbitrary starting structure until a self-similar or nearly self-similar evolving microstructure develops, which is what we do here starting from each lattice site being a unique orientation.

Our 2D simulation domain is discretized into 5000×5000 lattice points ($N_L = 2.5 \times 10^7$). We track the average grain size during the simulation using a linear intercept method. The average MC grain size can be characterized by a parameter L equal to the average number of lattice sites between grain boundaries along lines traversing the domain, which can be efficiently computed in parallel.

Figures 1(a) and (b) plots the evolving normalized grain size distribution for a 2D MC simulation run to average intercept distances of $L = 4, 8, 16, 32$ at zero and non-zero simulation temperatures, respectively. At zero simulation temperature, the distribution approaches a self-similar distribution slowly, and continues to evolve slightly as the grains grow. However, when the simulation temperature is set at the value suggested by Zöllner [30], the distribution appears nearly converged when the average intercept distance is only $L = 4$, and is not perceptibly changing after the intercept distance reaches $L = 8$. In all the remaining simulations, we use a non-zero simulation temperature as described in section 2.1. For our 2D test cases, we start with an initial microstructure where $L = 8$.

In the 3D example, our simulation domain is discretized into $700 \times 700 \times 200$ lattice points ($N_L = 9.8 \times 10^7$), and we initialize the simulation when the average intercept distance is $L = 4$ lattice sites. We start the 3D simulations with a smaller L because some of the grains

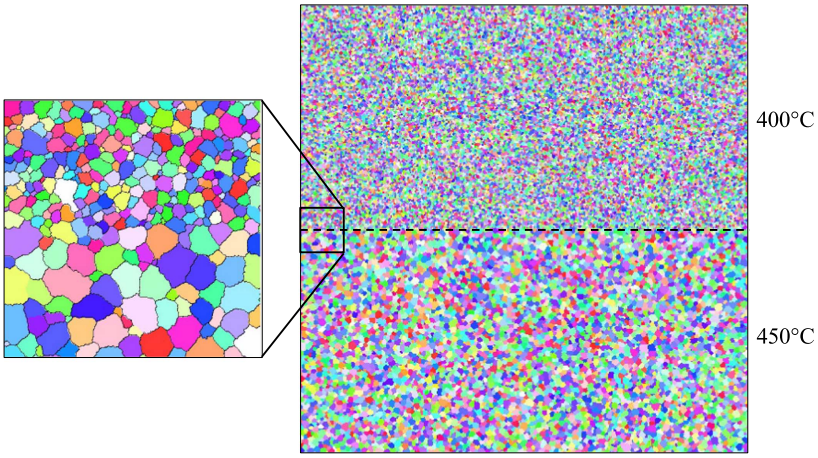

Figure 2. Simulation results for a copper thin film after 120 min of grain growth where the upper half of the domain is at 400 °C and the lower half is at 450 °C. Simulation domain 687.5 μm × 687.5 μm. Zoomed view of 1/10 of region spanning the centerline is shown on the left.

grow considerably during the simulation, and we want to ensure that we have multiple grains through the thickness of the domain, while keeping the number of lattice sites N_L to below 10^8. The 2D with $L = 8$ and the 3D with $L = 4$ normalized grain size distributions are shown in figure 1(c), where the simulation temperature is set as described in section 2.1. We can see that they are very close.

3.2. Test case 1: growth exponent $m \approx n = 2$

In this case, we model 2D copper grain growth fit to the experimental data for thin film copper by Gangulee [33]. Gangulee observed grain growth in 1μm thick copper films annealed at 400 °C, 450 °C, and 500 °C. He observed a grain growth exponent of $n = 2$, which matches the classic theory of Burke and Turnbull [41]. Likewise, the MC model with the given simulation conditions predicts a grain growth exponent of $m \approx 2$. In this case, as discussed in section 2.3, we expect our simulations to match those using the probability functions proposed by Godfrey and Martin [1] and Radhakrishnan and Zacharia [2]. In previous work, we directly compare our MC simulation to experimentally observed grain growth of a copper film undergoing a 30 min anneal at 350 °C in a scanning electron microscope [13]. In that work, we obtained grain size statistics that were in good agreement with slightly more uniform grains (lower standard deviation and kurtosis) predicted in the simulation than the experiment, likely due to not considering the effect of grain boundary anisotropy.

We use the 2D simulation domain described in section 3.1 with the lattice spacing assumed to be $\lambda = 0.1375$ μm for a simulation domain size of 687.5 μm × 687.5 μm. The average initial grain size was $\bar{D}_0 = 1.1$ μm, the same as in Gangulee's experiment [33]. The linear intercept method was used both in Gangulee and in this example for determining the average grain size $\bar{D}$ [42].

First, we fit the MC simulation results and reported experimental data to equations (3) and (4) for a uniform temperature field over the domain. The resulting parameters are listed in table 1. We did a least squares fit of our MC grain growth simulation to obtain m and C. The resulting grain growth exponent is $m = 2.12$, very close to the expected value of 2, with a

Table 1. Parameters fit to MC simulation and experiment [33] for test case 1.

Model parameter	λ (μm)	C	m	n	K (μm^2 s^{-1})	Q (kJ mol^{-1})
Value	0.1375	0.5282	2.12	2	9.43×10^7	146

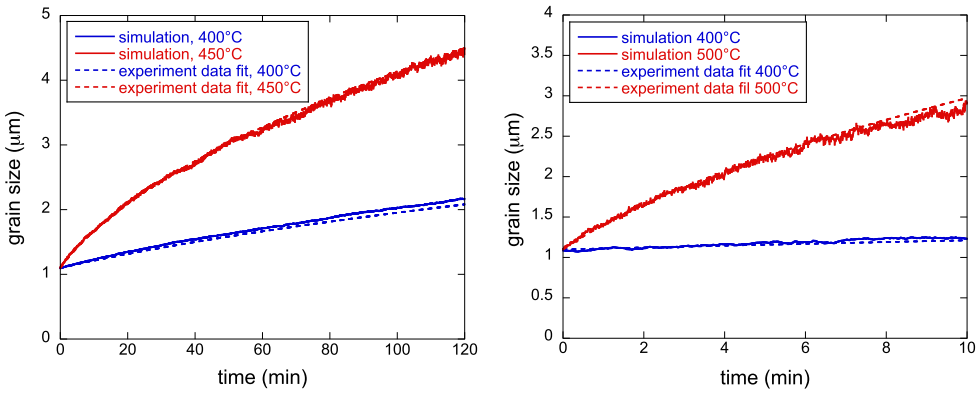

Figure 3. Comparison of fitted isothermal experimental [33] average grain size trajectory with the simulated average grain size evolution for a domain with regions at two different temperatures using the SSP function derived here (equation (14)). (a) 400 °C and 450 °C, average of five simulations shown. (b) 400 °C and 500 °C, one simulation shown.

95% confidence interval within 0.3% of this value. The 95% confidence interval for the grain growth coefficient C is within 1.7% of the value listed.

To verify the simulation with different temperatures in the domain, we split the 2D domain where the upper half was held at a constant temperature of 400 °C, while the lower half was at 450 °C. The initial grain size was again taken to be $D_0 = 1.1$ μm. The simulation was run to a physical time of $t = 120$ min. We expect each half to behave similar to the uniform temperature field case scaled to the appropriate temperature. From the fit to the experimental data, at the end of the simulation the average grain size should be 2.1 μm in the 400 °C region and 4.5 μm in the 450 °C region. Figure 2 shows the simulated grain structure at the end of a simulation using our SSP function (14). As expected, the grains are much larger in the region at the higher temperature. For a more quantitative analysis, we computed the average grain size in each temperature region of the simulation domain with the linear intercept method, excluding lattice points within 500λ from the center dashed line. We repeated the simulation five times with different random number seeds used in the MC simulations and compute the grain size at each time by averaging over the five simulations. Figure 3(a) shows the grain size evolution in each region compared to that expected from the isothermal case using the fit to Gangulee's experiment [33]. In addition to using our probability function, we ran simulations of the same case using the functions proposed by Godfrey and Martin [1] and Radhakrishnan and Zacharia [2]. The evolution of grain size was nearly identical for all three cases, which is in agreement with our analysis in section 2.3.

To demonstrate the algorithm for a larger temperature difference and also to show the result without averaging over multiple simulations, an additional simulation was performed

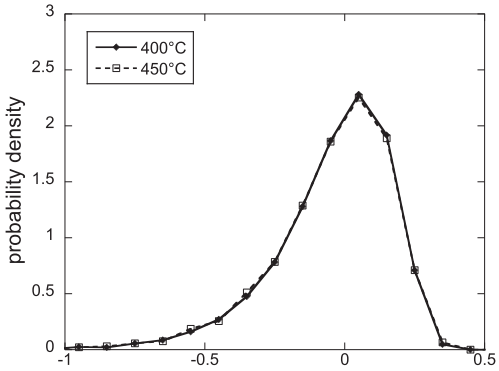

Figure 4. Grain size distributions after 120 min of grain growth.

Table 2. Parameters fit to MC simulation and experiment [35] for test case 2.

Model parameter	λ (nm)	C	m	n	K (μm^n s^{-1})	Q (kJ mol^{-1})
Value	3.75	0.5282	2.12	5.3	5.37	126.2

with the domain split into regions at 400 °C and 500 °C. The simulation was run to a physical time of $t = 10$ min, and the results are shown in figure 3(b). The results are in similar agreement to a single run of the 400 °C/450 °C case. We can see that when only a single simulation is used, the results are noisier than when averaged over five simulations as expected, but still in good agreement.

Figure 4 shows the normalized grain size distribution for the two parts of the domain, with the temperature at 400 °C and 450 °C, at the end of the simulation. The distributions are nearly identical and consistent with observations from experiments and other MC simulations for normal grain growth [5, 24]. This is to be expected since the normalized distribution is typically considered time invariant, and an increase in temperature affects the growth rate according to equation (4). Both distributions peak at $\log(D/\bar{D}) = 0$, which indicates that they peak at the average grain size. We also see that the distribution has an upper cut-off at $\log(D/\bar{D}) = 0.4$, which represents a maximum grain size of 2.5 times the average. The lower cut-off is more gradual, and the minimum grain size is approximately 0.04 times the average.

3.3. Test case 2: growth exponent $n \neq 2$

Here, we choose the experimental work by McBee *et al* [35] who studied grain growth in aluminum-4%copper (Al-4%Cu) films, where the grain growth exponent $n \neq 2$. McBee *et al* observed grain growth in 0.26 μm thick film Al-4%Cu films annealed at 400 °C, 450 °C, and 500 °C. Al-4%Cu forms non-coherent precipitates that inhibit grain growth resulting in a much lower grain growth rate than in pure aluminum. Fitting the data reported in McBee *et al* to the grain growth equation (4), we obtain the parameters listed in table 2, and notably a grain growth exponent of $n = 5.3$. In the simulation, we used the same initialized grain structure on a 5000 × 5000 lattice grid as for test case 1, except with lattice spacing scaled to $\lambda = 3.75$ nm to correspond to an initial average grain size of $\bar{D}_0 = 30$ nm, matching the initial reported grain size. As in case 1, we simulated a domain with two temperatures, 400 and 450 °C, held constant in each half of the domain.

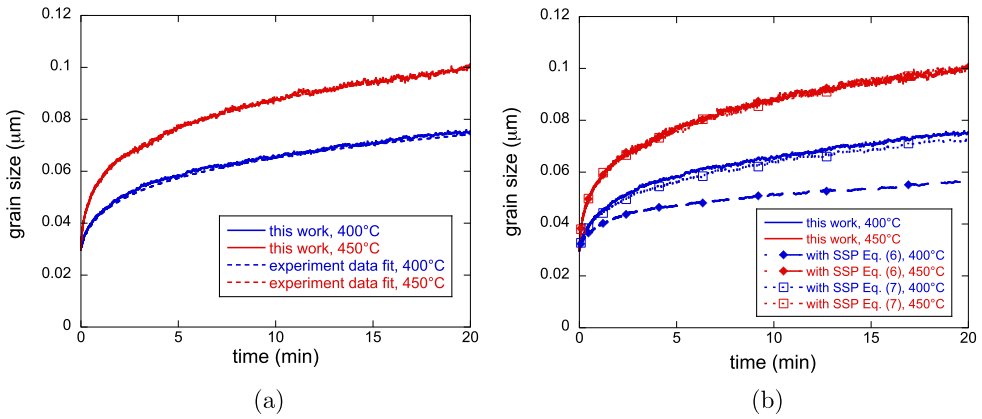

Figure 5. (a) Comparison of grain size between the fitted isothermal experimental [35] trajectory with the simulated results by using SSP function in this work, equation (14). (b) Comparison of simulated results using SSP functions in this work (equation (14)), Godfrey and Martin [1] (equation (6)) and Radhakrishnan and Zacharia [2] (equation (7)).

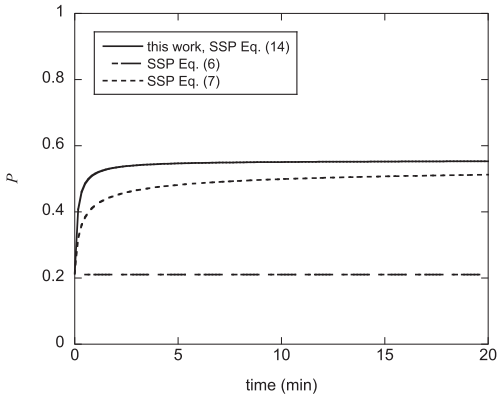

Figure 6. Evolution of SSP functions in the 400 °C region for test case 2 showing this work (equation (14)), Godfrey and Martin [1] (equation (6)) and Radhakrishnan and Zacharia [2] (equation (7)).

Figure 5(a) shows the simulation results compared to the expected curves from the fit to the isothermal experimental data in McBee *et al* [35], and figure 5(b) compares the results using the SSP defined in this work, equation (14), to the results predicted using the SSP functions of Godfrey and Martin [1], equation (6), and Radhakrishnan and Zacharia [2], equation (7). In the 450 °C region, the temperature is at the maximum temperature, and thus $P = 1$ for all three SSP. Thus, all three models give nearly the same results matching the experimental curve that the model is scaled to using equation (8). It is in the 400 °C region where the SSP functions are different resulting in different rates of grain growth. The SSP of Godfrey and Martin [1] significantly under predicts the expected grain size, while the SSP of Radhakrishnan and Zacharia [2] only slightly under predicts the expected grain size. The SSP introduced here is the closest fit to the expected grain size.

Table 3. Parameters fit to MC simulation and experiment [8, 43] for test case 3.

Model parameter	λ (μm)	C	m	n	K ($\mu m^n\ s^{-1}$)	Q (kJ mol^{-1})
Value	30	0.4553	1.92	1.84	3.30×10^9	170

Table 4. The parameters used in temperature equation (21) in test case 3.

Model parameter	T_0 (K)	q (W)	η	α ($mm^2\ s^{-1}$)	k (W mmK^{-1})	v (mm s^{-1})
Value	1248	2131	0.5	8.1967	0.020	1

To better understand these results, a graph showing the evolution of all three SSP functions in the 400 °C region is shown in figure 6. At the beginning of the simulation, the SSP functions reduce to the same equation and yields $P = 0.210$ initially. The SSP function of Godfrey and Martin [1], equation (6), depends only on the local temperature, and thus, does not evolve. The SSP function developed here, equation (14), and that proposed by Radhakrishnan and Zacharia [2], equation (7), tend to the same probability at long times $P(t \to \infty) = 0.555$, but in between, Radhakrishnan and Zacharia's SSP is less than the one presented in this work.

3.4. Test case 3: 3D welding

In this example, we model grain growth in the HAZ of a weld, where there is a large, time dependent temperature gradient. Several researchers [2, 8, 24, 27] have modeled grain growth in the HAZ during welding by using the SSP function of Radhakrishnan and Zacharia [2], equation (7). Here we simulate grain growth in the HAZ during gas tungsten arc welding of Ti-6Al-4V, which was modeled previously by Mishra and DebRoy [8]. We compared the prediction of our new SSP function, equation (14), with that using the SSP of Radhakrishnan and Zacharia [2].

As in the previous examples, we first must determine the parameters fitting the MC simulation and experimental data in equations (3) and (4), for uniform temperature fields. We use the 3D simulation domain described in section 3.1 with the lattice spacing assumed to be $\lambda = 30\ \mu$m for a simulation domain size of 21 mm × 21 mm × 6 mm, and average initial grain size was $D_0 = 120\ \mu$m. Fitting the MC equation (3) and using the grain growth parameters reported in [8] based on the experiments presented in [43], we obtain the parameters listed in table 3.

For the time dependent temperature field in our simulations, we used the following analytic approximation often used in welding [44, 45]

$$T(\boldsymbol{x}, t) = T_0 + \frac{q\eta}{2\pi k r(\boldsymbol{x})} \exp\left[-\frac{v(r(\boldsymbol{x}) - vt)}{2\alpha}\right], \tag{21}$$

where T_0 is the interpass temperature, q is the arc power, η is the arc efficiency, α is the thermal diffusivity, k is the thermal conductivity, and r is the initial distance a point at $\boldsymbol{x}$ is from the heat source moving with velocity magnitude v in the x_2 direction. The heat source moves from $(x_1, x_2, x_3) = (0, 0, 0)$ along the x_2 direction. Table 4 lists all the parameters used in computing the temperature field in equation (21), which are the same as or calculated from those in [8]. Here we take $T_0 = 1248$ K, which is the β-transus temperature, as we focus on

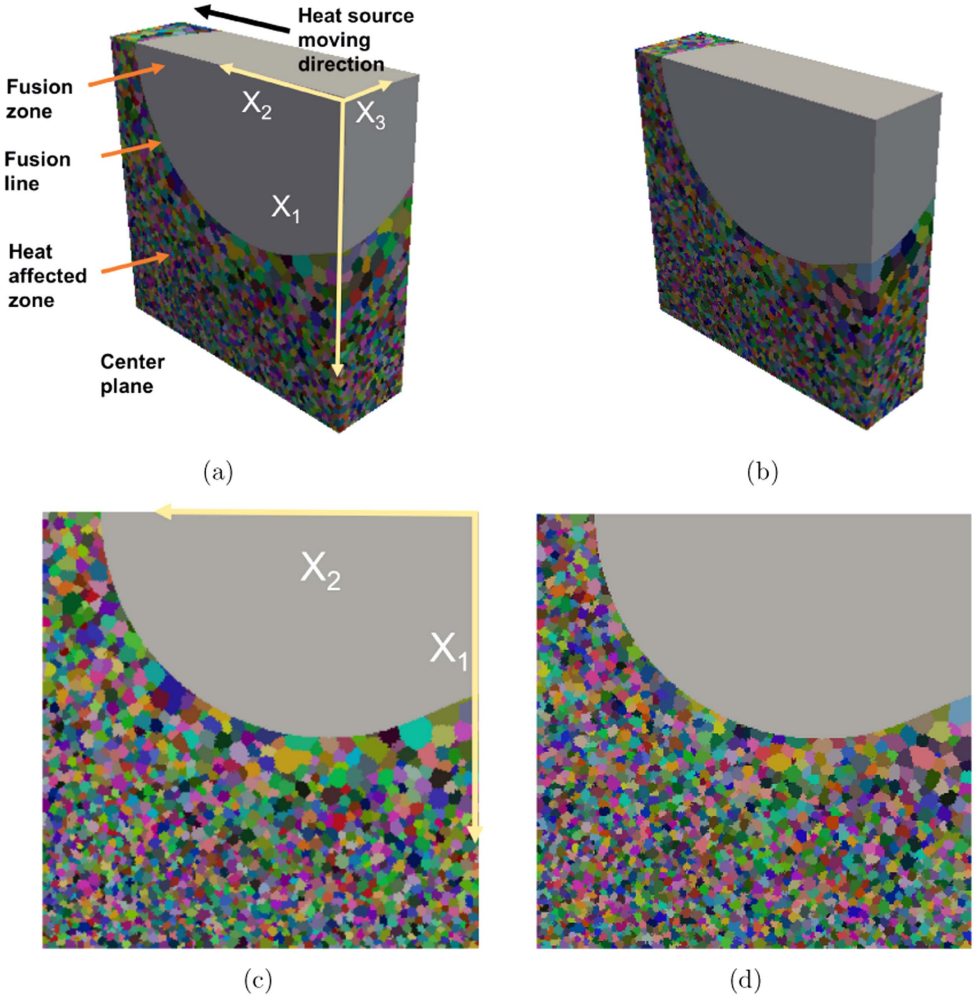

Figure 7. Simulated grain structure in the HAZ using (a) SSP function in this work, equation (14) and (b) Radhakrishnan and Zacharia [2] SSP function, equation (7). The center planes (x_1–x_2 plane at $x_3 = 0$) with SSP by (c) this work and (d) Radhakrishnan and Zacharia [2].

grain growth above the β-transus, when grain growth is much faster, and only a very small region close to the weld. The solidus temperature is $T_s = 1878$ K. The region above the solidus temperature is the fusion zone. The whole thermal cycle is broken into a sequence of short iso-thermal steps at different times with step size Δt determined by constraint condition $\Delta t_{\mathrm{mc}}(\boldsymbol{x}^*) = 1$. We found that $\Delta t_{\max} = 0.00119s$, which is sufficiently small to accurately model the temperature history. Each simulation ran to $\max(t_{\mathrm{mc}}) = 7400$ and grain growth time $t \approx 7.5$ s.

The simulated grain structure after welding for 7.5 s are shown in figure 7. We can see that the SSP function of Radhakrishnan and Zacharia [2] in equation (7) results in smaller grains at the same locations than using the SSP function defined in this work in equation (14). For a more quantitative analysis, we repeated the simulation five times and computed the

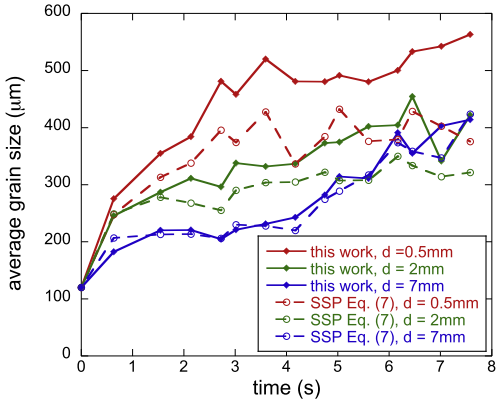

Figure 8. Comparison of the evolution of average grain size using the SSP from this work, equation (14), and that of Radhakrishnan and Zacharia [2], equation (7), at different distances, d, from the fusion zone on the center plane (x_1–x_2 plane at $x_3 = 0$).

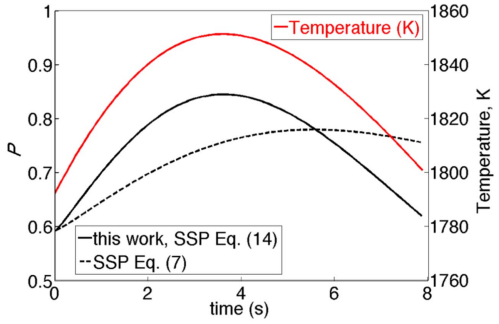

Figure 9. Comparison of the evolution of SSP at $(x_1, x_2, x_3) = (9\text{ mm}, 0, 0)$ between the simulation using SSP functions in this work, equation (14), and in Radhakrishnan and Zacharia [2], equation (7), and the temperature history at $(x_1, x_2, x_3) = (9\text{ mm}, 0, 0)$.

average grain size at various distances from the boundary of the fusion zone on the center plane. That result is plotted in figure 8. Further from the fusion zone, where the grains are growing more slowly, there is little difference between the simulations, however, close to the fusion zone, where the grains are growing very quickly, we see a very large difference in the average grain size with the grains using the SSP from this work roughly 50% larger at the end of the simulation than those predicted using the SSP of Radhakrishnan and Zacharia.

To better understand why the grain size is so different for the different simulations, a graph showing the temperature history and each of the SSP functions evaluated at a location near the fusion zone $(x_1, x_2, x_3) = (9\text{ mm}, 0, 0)$ is plotted in figure 9. We see that the SSP function from this work, equation (14), is much higher than the SSP function in equation (7) in the earlier stages of the simulation, and more closely tracks the temperature history. The SSP function in equation (14) closely tracks the temperature history because the first term in the product, which dominates, is

$$\frac{\exp\left(-\frac{Q}{RT(x)}\right)}{\exp\left(-\frac{Q}{RT(x^*)}\right)}. \tag{22}$$

On the other hand, the Radhakrishnan and Zacharia [2] SSP function in equation (7) tends to lag because it uses the current accumulated MC step t_{mc} in computing the SSP instead of the differential used in the derivation of the SSP here based on equation (12). To see this let $n \approx m$, which is true in this example. Equating equations (3) and (5) yields

$$t_{mc} = \frac{K}{C\lambda^m}\int_0^t \exp\left(-\frac{Q}{RT(t')}\right)dt' \tag{23}$$

which is used to define the SSP P in equation (7).

4. Conclusion

This work provides a theoretical derivation for a SSP function for use in MC simulation of grain growth in the presence of a non-uniform, time varying temperature field. We compare our new SSP function with two others in the literature [1, 2]. The main conclusions are:

(i) The SSP function in equation (6) (Godfrey and Martin [1]) matches the SSP function derived here, equation (14), when the physical grain growth exponent matches the MC simulation growth exponent, $n = m$.
(ii) The SSP function in equation (7) (Radhakrishnan and Zacharia [2]), widely used in the welding community, matches our newly proposed SSP function in equation (14) when the temperature field is not time dependent and when either $n = m$ or $D \gg D_0$.
(iii) In the simple 2D test cases presented here, we demonstrate the two conclusions above and show that when $n \neq m$ the SSP function derived herein more accurately follows the expected average grain size evolution in a region with a homogeneous, constant temperature field.
(iv) For the more general test case of simulating the HAZ in the vicinity of a weld, with the temperature field changing in both time and space, we find the results of our new SSP function more closely tracks the temperature field history than the SSP of Radhakrishnan and Zacharia [2], which is expected because the SSP is derived here based on the differential MC step rather than the current accumulated MC step.

The SSP function proposed in this work is promising for MC simulation of grain growth during various material manufacturing processes, e.g. welding, laser melting, sintering, where strong local temperature gradients and/or thermal cycles exist.

Acknowledgments

This research is sponsored through a grant from the National Science Foundation, Award CMMI-1334283, DMREF: Real Time Control of Grain Growth in Metals. The authors acknowledge our co-workers on this grant, Profs Robert Hull and Dan Lewis, and graduate students David Christ and Genevieve Kane. The authors also deeply thank Dr Trevor Keller for his valuable suggestion on programming issues. The simulations presented were carried out on the Blue Gene/Q at the Center for Computational Innovations at Rensselaer.

References

[1] Godfrey A and Martin J 1995 Some Monte Carlo studies of grain growth in a temperature gradient *Phil. Mag.* A **72** 737–49

[2] Radhakrishnan B and Zacharia T 1995 Monte Carlo simulation of grain boundary pinning in the weld heat-affected zone *Metall. Mater. Trans.* A **26** 2123–30

[3] Humphreys F and Hatherly M 2004 *Recrystallization and Related Annealing Phenomena* 2nd edn (Oxford: Elsevier)

[4] Anderson M, Srolovitz D, Grest G and Sahni P 1984 Computer simulation of grain growth: I. Kinetics *Acta Metall.* **32** 783–91

[5] Srolovitz D, Anderson M, Sahni P and Grest G 1984 Computer simulation of grain growth: II. Grain size distribution, topology, and local dynamics *Acta Metall.* **32** 793–802

[6] Gao J and Thompson R 1996 Real time-temperature models for Monte Carlo simulations of normal grain growth *Acta Mater.* **44** 4565–70

[7] Yu Q and Esche S K 2003 Three-dimensional grain growth modeling with a Monte Carlo algorithm *Mater. Lett.* **57** 4622–6

[8] Mishra S and DebRoy T 2004 Measurements and Monte Carlo simulation of grain growth in the heat-affected zone of Ti-6Al-4V welds *Acta Mater.* **52** 1183–92

[9] Yue X, Feng X L and Lippold J 2014 Effect of welding parameters on the heat-affected zone hydrogen-induced cracking tendency of a blast-resistant steel *Weld. J.* **93** 98s–105s

[10] Badmos A, Frost H and Baker I 2002 Microstructural evolution during directional annealing *Acta Mater.* **50** 3347–59

[11] Zheng C, Balasubramanian P, Tan Y, Maniatty A M, Hull R and Wen J T 2017 Simulation, microfabrication and control of a micro-heater array *IEEE/ASME Trans. Mechatronics* 1–6

[12] Zheng C, Tan Y, Wen J T and Maniatty A M 2015 Finite element model based temperature consensus control for material microstructure *American Control Conference (ACC), 2015* (Piscataway, NJ: IEEE) pp 619–24

[13] Balasubramanian P *et al* 2016 Substrates with programmable heater arrays for dynamic control of the microstructure of polycrystalline films: towards real time control of grain growth in metals *MRS Adv.* **26** 1947–52

[14] Srolovitz D, Anderson M, Grest G and Sahni P 1984 Computer simulation of grain growth: III. Influence of a particle dispersion *Acta Metall.* **32** 1429–38

[15] Grest G, Srolovitz D and Anderson M 1985 Computer simulation of grain growth: IV. Anisotropic grain boundary energies *Acta Metall.* **33** 509–20

[16] Yu Q, Nosonovsky M and Esche S K 2009 Monte Carlo simulation of grain growth of single-phase systems with anisotropic boundary energies *Int. J. Mech. Sci.* **51** 434–42

[17] Fjeldberg E and Marthinsen K 2010 A 3D Monte Carlo study of the effect of grain boundary anisotropy and particles on the size distribution of grains after recrystallisation and grain growth *Comput. Mater. Sci.* **48** 267–81

[18] Allen J B, Cornwell C F, Devine B D and Welch C R 2013 Simulations of anisotropic grain growth subject to thermal tradients using *Q*-State Monte Carlo *J. Eng. Mater. Technol.* **135** 041005

[19] Rollett A, Srolovitz D J and Anderson M 1989 Simulation and theory of abnormal grain growth. Anisotropic grain boundary energies and mobilities *Acta Metall.* **37** 1227–40

[20] Grest G, Anderson M, Srolovitz D and Rollett A 1990 Abnormal grain growth in three dimensions *Acta Metall. Mater.* **24** 661–5

[21] Raabe D 2000 Scaling Monte Carlo kinetics of the Potts model using rate theory *Acta Mater.* **48** 1617–28

[22] Zhang L, Rollett A D, Bartel T, Wu D and Lusk M T 2012 A calibrated Monte Carlo approach to quantify the impacts of misorientation and different driving forces on texture development *Acta Mater.* **60** 1201–10

[23] Nosonovsky M, Zhang X and Esche S K 2009 Scaling of Monte Carlo simulations of grain growth in metals *Modelling Simul. Mater. Sci. Eng.* **17** 025004

[24] Yang Z, Sista S, Elmer J and DebRoy T 2000 Three dimensional Monte Carlo simulation of grain growth during GTA welding of titanium *Acta Mater.* **48** 4813–25

[25] Zacharopoulos N, Holm E A and Srolovitz D J 1995 Simulation of grain growth during directional annealing *Mater. Res. Soc. Symp. Proc.* **362** 271–6

[26] Garcia A L, Tikare V and Holm E A 2008 Three-dimensional simulation of grain growth in a thermal gradient with non-uniform grain boundary mobility *Scr. Mater.* **59** 661–4
[27] Shi Y, Chen D, Lei Y and Li X 2004 HAZ microstructure simulation in welding of a ultra fine grain steel *Comput. Mater. Sci.* **31** 379–88
[28] Zhang Z and Wu C 2012 Monte Carlo simulation of grain growth in heat-affected zone of 12 wt.% Cr ferritic stainless steel hybrid welds *Comput. Mater. Sci.* **65** 442–9
[29] Holm E, Glazier J, Srolovitz D and Grest G 1991 Effects of lattice anisotropy and temperature on domain growth in the two-dimensional Potts model *Phys. Rev.* A **43** 2662–8
[30] Zöllner D 2014 A new point of view to determine the simulation temperature for the Potts model simulation of grain growth *Comput. Mater. Sci.* **86** 99–107
[31] Gruber J, Miller H M, Hoffmann T D, Rohrer G and Rollett A D 2009 Misorientation texture development during grain growth: I. Simulation and experiment *Int. J. Mech. Sci.* **51** 434–42
[32] Upmanyu M *et al* 2002 Boundary mobility and energy anisotropy effects on microstructural evolution during grain growth *Interface Sci.* **10** 201–16
[33] Gangulee A 1974 Structure of electroplated and vapor-deposited copper films: III. Recrystallization and grain growth *J. Appl. Phys.* **45** 3749–56
[34] Semiatin S, Soper J and Sukonnik I 1996 Short-time beta grain growth kinetics for a conventional titanium alloy *Acta Mater.* **44** 1979–86
[35] Mcbee W C and McComb J A 1975 Grain growth in thin aluminum-4% copper alloy films *Thin Solid Films* **30** 137–43
[36] Iordache M, Whang S, Jiao Z and Wang Z 1999 Grain growth kinetics in nanostructured nickel *Nanostruct. Mater.* **11** 1343–9
[37] Wright S A, Plimpton S J, Swiler T P, Fye R M, Young M F and Holm E A 1997 Potts-model grain growth simulations: parallel algorithms and applications *SAND Report* SAND97–1925 p 1925
[38] Gruber J and Keller T The mesoscale microstructure simulation project https://github.com/mesoscale/mmsp
[39] Mullins W W 1986 The statistical self-similarity hypothesis in grain growth and particle coarsening *J. Appl. Phys.* **59** 1341–9
[40] Zöllner D, Streitenberger P and Rios P R 2016 Shedding some light on the early grain growth regime: About the effect of the initial microstructure on normal grain growth *Comput. Mater. Sci.* **113** 11–20
[41] Burke J E and Turnbull D 1952 Recrystallization and grain growth *Prog. Met. Phys.* **3** 220–92
[42] Abrams H 1971 Grain size measurement by the intercept method *Metallography* **4** 59–78
[43] Gil F J, Tarin P and Planell J A 1992 Grain growth kinetics in beta phase Ti-6Al-4V alloy *Titanium '92: Science and Technology* vol 1 ed F H Froes and I L Caplan (Warrendale, PA: TMS) pp 777–84
[44] Handbook W 2001 *Weld. Sci. Technol.* **1** 452–82
[45] Sista S, Yang Z and DebRoy T 2000 Three-dimensional Monte Carlo simulation of grain growth in the heat-affected zone of a 2.25Cr-1Mo steel weld *Metall. Mater. Trans.* B **31B** 529–36